Int J Adv Manuf Technol (2013) 69:1483–1497
DOI 10.1007/s00170-013-5094-7

ORIGINAL ARTICLE

A general strategy for geometric error identification of multi-axis machine tools based on point measurement

Zhenjiu Zhang · Hong Hu

Received: 27 December 2012 / Accepted: 27 May 2013 / Published online: 25 June 2013
© Springer-Verlag London 2013

Abstract Geometric error component identification is needed to realize the geometric error compensation which can significantly enhance the accuracy of multi-axis machine tools. Laser tracker has been applied to geometric error identification of machine tools increasingly due to its high capability in 3D metrology. A general method, based on point measurement using a laser tracker is developed for identifying the geometric error components of multi-axis machine tools in this study. By using this method, all the component errors and location errors of each axis (including the linear axis and rotary axis) of the multi-axis machine tools can be measured. Three pre-described targets are fixed on the stage of the under-test axis which moves step by step. The coordinates of the three targets at every step are determined by a laser tracker based on the sequential multilateration method. The volumetric errors of these three target points at each step can be obtained by comparing the measured values of the target points' coordinates with the ideal values. Then, nine equations can be established by inversely applying the geometric error model of the axis under test, which can explicitly describe the relationship between the geometric error components and volumetric error components, and then the component errors of this axis can be obtained by solving these equations. The location errors of the axis under test can be determined through the curve fitting. In brief, all the geometric error components of a single axis of multi-axis machine tools can be measured by the proposed method. The validity of the proposed method is verified through a series of experiments, and the experimental results indicate that the proposed method is capable of identifying all the geometric error components of multi-axis machine tools of arbitrary configuration.

Z. Zhang · H. Hu (✉)
Department of Mechanical Engineering and Automation, Harbin Institute of Technology Shenzhen Graduate School, Shenzhen, Guangdong province 518055, China
e-mail: honghu@hit.edu.cn

Keywords Machine tools · Error compensation · Geometric error measurement · Sequential multilateration principle · Laser tracker

1 Introduction

Multi-axis machine tools have been widely used in industrial production due to their high efficiency and capability in machining [1–3]. Accuracy is a crucial consideration for evaluating the capability of multi-axis machine tools. Geometric error is one of the key contributors to the overall errors of machine tools. Many researchers have focused on research into geometric error compensation [4–6]. Therefore, as the basis of the geometric error compensation, geometric error identification methods have necessarily been developed.

Many commercial devices can be used to measure the geometric errors of multi-axis machine tools. Laser interferometer, which can only measure linear displacement error, can be applied to identify all the 21 geometric error components by measuring the positioning errors along 22 lines, 15 lines, 14 lines, nine lines, body diagonals, or step diagonals within the workspace of three-axis machine tools [7–12]. The laser interferometer can also directly detect all the six geometric error components of the linear axis and the rotary axis associated with prismatic joints, 6D sensors, rotary axis calibrators, multi-face mirrors, and other devices, such as capacitive transducers and electronic levels, etc. [13–15]. These laser-interferometer-based approaches have high accuracy, but the measurement for each linear axis or each line has to be done in turn, the error components of rotary axis has to be identified with several different accessories, so that the setup needs to be re-installed many times. Moreover, the installation and calibration of the measuring system is always complicated for large machine tools. In conclusion, the laser-interferometer-based approaches have some disadvantages,

such as the long calibration time and the requirement for experienced operator. Other commercial devices, such as the double ball bar (DBB) and cross-grid encoder, can be applied to evaluate the geometric error components of multi-axis machine tools. The DBB was proposed by Bryan in 1982 [16, 17], and it is used to measure the geometric error of multi-axis machine tools [18–21]. The DBB-based methods are economical and they are particularly simple to acquire data. However, due to the size of the DBB, it can never cover the whole work space of a machine tool, especially for the large machine tools. In addition, the DBB cannot measure the angular positioning error of the rotary axis. The cross-grid encoder is a precision device for two-dimensional (2D) position measurement, and many methods have been proposed to measure the geometric error of machine tools using a cross-grid encoder [22, 23]. These methods are simple and efficient. However, the measuring range of these methods is limited by the size of the grid encoder, so that it is also not suitable for geometric error measurement of large-sized machine tools. In addition, it cannot be used to measure the geometric errors of the rotary axis.

Many special measuring systems have been developed for identifying the geometric errors of multi-axis machine tools. Wang et al. developed a measuring system consisting of laser diodes, beam splitters, and 2D position sensing detectors to measure the geometric error components of three-axis machine tools [24]. Liu et al. developed a measuring system using a diffraction grating, a laser diode, and position-sensitive detectors to measure the error motions of an indexing table [25]. Sung-Ryung Park developed an optical measurement system with a laser diode, two position-sensitive detectors, beam splitters, and a turning mirror to measure the six geometric errors of a rotary axis separately [26]. These measuring systems have high performance. However, each of them is only suitable for a linear axis or a rotary axis or machine tools of a particular type.

Laser tracker is increasingly used to identify the geometric errors of machine tools due to its capability of measuring 3D coordinates. Multilateration and sequential multilateration methods have been developed and studied to enhance the accuracy of 3D coordinate measurement, so that the laser tracker can meet the accuracy requirement for calibrating machine tools [27–30]. Kenta Umetsu et al. identified all the geometric error components of three-axis machine tools by using multilateration to allocate the measured points on 21 lines in the six planes of the work space [30]. This method has a high cost since four laser trackers are involved. The measurement is conducted on up to 21 lines, so that it is time consuming. Researchers have made use of sequential multilateration which requires only one laser tracker to calibrate multi-axis machine tools [29, 31–34]. Due to the utilization of sequential multilateration, the cost of such a measuring system is greatly reduced. Based on sequential multilateration or multilateration principle, the displacement approaches can determine the geometric error components of the linear axis [31, 32]. However, these displacement approaches are not suitable for testing the rotary axis because only the error models for the linear axis can be used in combination with the displacement approaches. Point measurement can be applied to detect the volumetric errors of the sample points, and then the volumetric errors can be used to identify the geometric error components of the linear axis and the rotary axis of machine tools or the parameters of error models [29, 33, 34]. The laser tracker has to be placed on the turntable when testing the rotary axis by using point measurement approaches, so that these methods are only suitable for a rotary axis with a large-sized turntable. In addition, numerous sample nodes have to be tested while using these approaches to test the linear axis, which will lead to relative long measurement time.

In view of the limitations stated, this paper presents a general method for measuring the geometric error of multi-axis machine tools. This method is suitable for both linear and rotary axes, and it can further decrease the measurement time due to the requirement that only three point sequences are tested. The rest of this paper is organized as follows: In Section 2, the geometric error model of a single linear axis and a single rotary axis are presented. In Section 3, the sequential multilateration method for measuring 3D coordinates is introduced. Section 4 presents a three-point method for geometric error measurement of linear and rotary axes based on 3D coordinate measurement. In Section 5, the experiments are demonstrated to validate the proposed three-point method. Section 6 addresses the conclusions and summary.

2 Error model of the linear axis and the rotary axis

2.1 Error model of the linear axis

Taking the x-slide as an example, the error model of the linear axis is introduced in this section. The linear axis stage can be considered as a rigid body. It is known that a unconstrained moving rigid body has six degree of freedoms, therefore, the x-slide has six geometric error components: three displacement errors, i.e., straightness errors $\delta_y(x)$, $\delta_z(x)$, and linear error $\delta_x(x)$, and three rotational errors, i.e., roll error $\varepsilon_x(x)$, pitch, and yaw errors $\varepsilon_y(x)$, $\varepsilon_z(x)$. All error components are the functions of the displacement of the x-slide. As shown in Fig. 1, $oxyz$ is the reference coordinate frame and $o_x x_x y_x z_x$ is the x-axis coordinate frame. The position of x-axis coordinate frame is changed by the displacement of x-slide and the error components. The relationship between these two coordinate frames can be derived by a 4×4

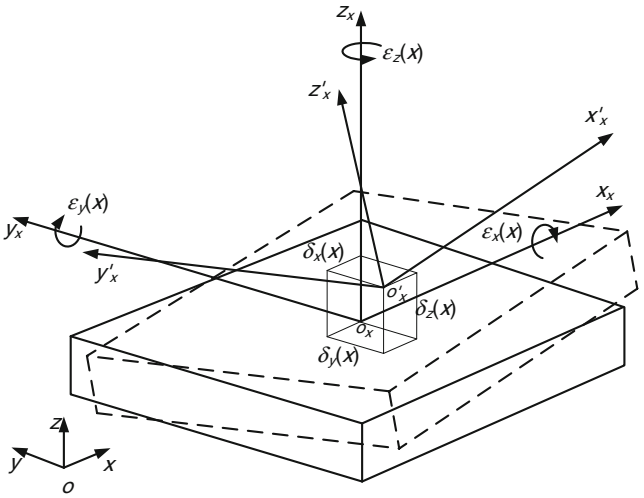

Fig. 1 Geometric error components of the linear axis

homogeneous transform matrix (HTM), and the volumetric error of a point P is given as [7]

$$\begin{bmatrix} \Delta_x(x) \\ \Delta_y(x) \\ \Delta_z(x) \\ 0 \end{bmatrix} = \begin{bmatrix} 0 & -\varepsilon_z(x) & \varepsilon_y(x) & \delta_x(x) \\ \varepsilon_z(x) & 0 & -\varepsilon_x(x) & \delta_y(x) \\ -\varepsilon_y(x) & \varepsilon_x(x) & 0 & \delta_z(x) \\ 0 & 0 & 0 & 0 \end{bmatrix} \begin{bmatrix} x_x \\ y_x \\ z_x \\ 1 \end{bmatrix} \quad (1)$$

where $\Delta_x(x)$, $\Delta_y(x)$, and $\Delta_z(x)$ are the volumetric errors, (x_x, y_x, z_x) is the coordinate of point P in the x-axis coordinate frame, and the x in parentheses denotes the displacement of x-slide.

From Eq. 1, we can get

$$\begin{cases} \Delta_x(x) = -y_x\varepsilon_z(x) + z_x\varepsilon_y(x) + \delta_x(x) \\ \Delta_y(x) = x_x\varepsilon_z(x) - z_x\varepsilon_x(x) + \delta_y(x) \\ \Delta_z(x) = -x_x\varepsilon_y(x) + y_x\varepsilon_x(x) + \delta_z(x) \end{cases} \quad (2)$$

Equations 1 and 2 are the error models of the linear axis. Obviously, the three volumetric error components of a point are not only related to the six geometric error components, but also related to the coordinates in the coordinate frame of the moving stage.

2.2 Error model of the rotary axis

Similar to the error analysis of the linear axis, the rotational motion of the rotary axis leads to six geometric error components. As shown in Fig. 2, $oxyz$ is the reference coordinate frame and $o_Cx_Cy_Cz_C$ is the C-axis (z-turntable) coordinate frame.

HTM is used to obtain Eq. 3, where the error model of rotary axis [20] is

$$\begin{bmatrix} \Delta_x(\theta) \\ \Delta_y(\theta) \\ \Delta_z(\theta) \\ 0 \end{bmatrix} = \begin{bmatrix} -\varepsilon_z(\theta)\sin\theta & -\varepsilon_z(\theta)\cos\theta & \varepsilon_y(\theta) & \delta_x(\theta) \\ \varepsilon_z(\theta)\cos\theta & -\varepsilon_z(\theta)\sin\theta & -\varepsilon_x(\theta) & \delta_y(\theta) \\ -\varepsilon_y(\theta)\cos\theta + \varepsilon_x(\theta)\sin\theta & \varepsilon_y(\theta)\sin\theta + \varepsilon_x(\theta)\cos\theta & 0 & \delta_z(\theta) \\ 0 & 0 & 0 & 1 \end{bmatrix} \begin{bmatrix} x_C \\ y_C \\ z_C \\ 1 \end{bmatrix} \quad (3)$$

where $\delta_y(\theta)$ and $\delta_z(\theta)$ are the radial displacement errors, $\delta_z(\theta)$ is the axial displacement error, $\varepsilon_x(\theta)$ and $\varepsilon_y(\theta)$ are the tilt errors, $\varepsilon_z(\theta)$ is the angular error, and θ is the angular displacement about the z-axis. All the error components are functions of the angular displacement θ.

From Eq. 3, we can get

$$\begin{cases} \Delta_x(\theta) = -\varepsilon_z(\theta)(x_C\sin\theta + y_C\cos\theta) + \varepsilon_y(\theta)z_C + \delta_x(\theta) \\ \Delta_y(\theta) = \varepsilon_z(\theta)(x_C\cos\theta - y_C\sin\theta) - \varepsilon_x(\theta)z_C + \delta_y(\theta) \\ \Delta_z(\theta) = \left[-\varepsilon_y(\theta)\cos\theta + \varepsilon_x(\theta)\sin\theta\right]x_C + \left[\varepsilon_y(\theta)\sin\theta + \varepsilon_x(\theta)\cos\theta\right]y_C + \delta_z(\theta) \end{cases} \quad (4)$$

3 3D coordinates measurement using a laser tracker

Laser tracker is a portable and large-scale instrument for 3D coordinate measurement based on a spherical coordinate system, but the capability of 3D coordinate measurement is limited by the accuracy of the angle measurement. Many researchers have developed the multilateration principle to realize 3D coordinates measurement with high accuracy [30]. However, there are totally four laser trackers used in the multilateration principle, which leads to an extremely high cost in such a measuring system. In this paper, a sequential multilateration principle presented in the literature [29] is applied to detect the 3D coordinates using a laser tracker.

By using the method mentioned in literature [30], the incremental length measurement accuracy of the FARO laser tracker is tested by comparison with a reference coordinate measuring machine. The maximum deviation and the repeatability are found to be 0.807 and 0.334 μm. The Monte Carlo method is then performed in two cases to evaluate the measurement uncertainty of the sequential multilateration method.

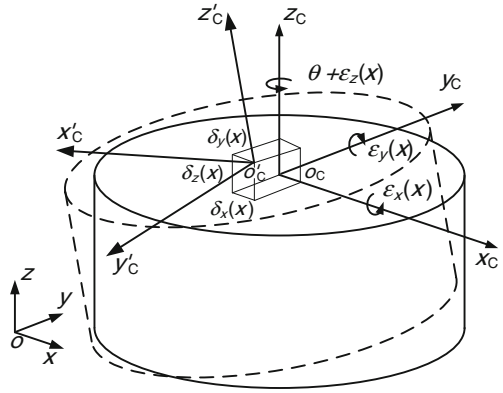

Fig. 2 Geometric error components of the rotary axis

According to the 3σ criterion, a normal distribution is assigned to these incremental lengths with zero expectation and standard deviation of 0.269 μm; assume that the positioning errors of the machine tool obeys random normal distributions within [0, 3 μm] in case 1 and [0, 5 μm] in case 2, respectively. All the points under test are located in the measurement volume of the measuring system which is of an optimal arrangement [30]. The number of simulation trials is 10,000. The simulation results are tabulated in Table 1, and the uncertainties of *x*, *y*, and *z* are quantified by maximum standard deviation with respect to the number of simulation trials for all the under-test points. According to the simulation results, the sequential multilateration measuring system has a much higher accuracy than most machine tools, thus, this method can be used to calibrate machine tools. We also can conclude that the uncertainty is remarkably improved after averaging the measurement results of *x*, *y*, and *z* obtained by repeating the experiment 10 times. Thus, in practical experiments, all the 3D coordinate measurements are repeated 10 times.

Table 1 Measuring errors obtained by simulation

	Number of repeat trials	Measurement uncertainty/μm		
		x	*y*	*z*
Case 1	1	1.27	1.33	1.29
	10	0.35	0.41	0.43
Case 2	1	2.03	1.97	2.14
	10	0.64	0.71	0.67

4 Method for geometric error measurement

4.1 Component error measurement for a single axis of multi-axis machine tool

4.1.1 Geometric error measurement for the linear axis

The *x*-slide is tested as an example to demonstrate the method for measuring geometric error components of the linear axis [35]. As shown in Fig. 3, *oxyz* is the reference coordinate frame. $o_x x_x y_x z_x$ is the *x*-axis coordinate frame, and it moves with the stage of *x*-slide. Three noncollinear points, *P*, *Q*, and *K* are fixed on the stage of an *x*-slide, and their coordinates in $o_x x_x y_x z_x$ are (x_{xP}, y_{xP}, z_{xP}), (x_{xQ}, y_{xQ}, z_{xQ}), and (x_{xK}, y_{xK}, z_{xK}) respectively. The *x*-slide moves step by step.

At the beginning, the homogeneous coordinates of o_x are $[x_o, y_o, z_o, 1]^T$ in the reference coordinate frame. The *x*-slide moves step by step. It is assumed that no errors occur while the *x*-slide is traveling. At step *t*, the displacement of *x*-slide is *x*, and the homogeneous coordinates of o_x is $[x_{ot}, y_{ot}, z_{ot}, 1]^T$ which can be obtained by

$$\begin{bmatrix} x_{ot} \\ y_{ot} \\ z_{ot} \\ 1 \end{bmatrix} = \begin{bmatrix} 1 & 0 & 0 & x \\ 0 & 1 & 0 & 0 \\ 0 & 0 & 1 & 0 \\ 0 & 0 & 0 & 1 \end{bmatrix} \begin{bmatrix} x_o \\ y_o \\ z_o \\ 1 \end{bmatrix} \tag{5}$$

Meanwhile, the homogeneous coordinates of point *P* is $[x_{Pt}, y_{Pt}, z_{Pt}]^T$ in the reference coordinate frame, and they can be obtained by

$$\begin{bmatrix} x_{Pt} \\ y_{Pt} \\ z_{Pt} \\ 1 \end{bmatrix} = \begin{bmatrix} 1 & 0 & 0 & x_{ot} \\ 0 & 1 & 0 & y_{ot} \\ 0 & 0 & 1 & z_{ot} \\ 0 & 0 & 0 & 1 \end{bmatrix} \begin{bmatrix} x_{xP} \\ y_{xP} \\ z_{xP} \\ 1 \end{bmatrix} \tag{6}$$

However, in practice, the movement of the *x*-slide will inevitably lead to geometric errors. The 3D coordinates of point *P* will be necessarily influenced by the geometric errors. The actual coordinates of *P* are $(x'_{Pt}, y'_{Pt}, z'_{Pt})$ which can be collected by a laser tracker and the corresponding homogeneous coordinates are $[x'_{Pt}, y'_{Pt}, z'_{Pt}, 1]$. The three

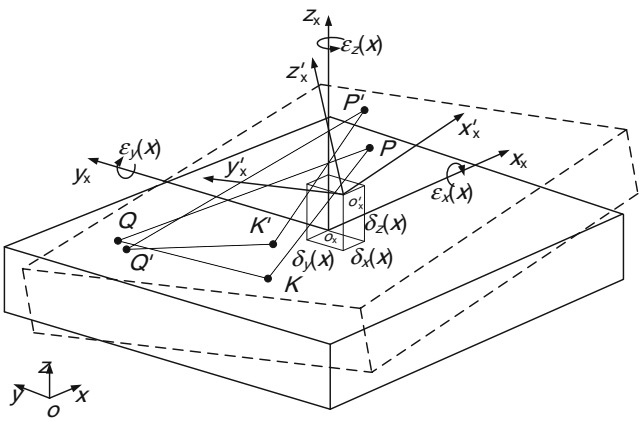

Fig. 3 Geometric error components measurement of *x*-slide

volumetric error components at point P are Δ_{Pxt}, Δ_{Pyt} and Δ_{Pzt}. By using Eqs. 5 and 6, we give

$$\begin{bmatrix} \Delta_{Pxt} \\ \Delta_{Pyt} \\ \Delta_{Pzt} \\ 0 \end{bmatrix} = \begin{bmatrix} x'_{Pt} \\ y'_{Pt} \\ z'_{Pt} \\ 1 \end{bmatrix} - \begin{bmatrix} x_{Pt} \\ y_{Pt} \\ z_{Pt} \\ 1 \end{bmatrix} = \begin{bmatrix} x'_{Pt} - x_{xP} - x_o - x \\ y'_{Pt} - y_{xP} - y_o \\ z'_{Pt} - z_{xP} - z_o \\ 0 \end{bmatrix} \tag{7}$$

Substitute Eq. 7 into Eq. 2, we give

$$\begin{cases} \Delta_{Pxt} = -y_{xP}\varepsilon_{zt}(x) + z_{xP}\varepsilon_{yt}(x) + \delta_{xt}(x) \\ \Delta_{Pyt} = x_{xP}\varepsilon_{zt}(x) - z_{xP}\varepsilon_{xt}(x) + \delta_{yt}(x) \\ \Delta_{Pzt} = -x_{xP}\varepsilon_{yt}(x) + y_{xP}\varepsilon_{xt}(x) + \delta_{zt}(x) \end{cases} \tag{8}$$

The same analysis procedure can be performed on points Q and K to give other six equations. Thus, there are totally nine equations, and they can be rewritten as

$$\begin{bmatrix} 1 & 0 & 0 & 0 & z_{xP} & -y_{xP} \\ 0 & 1 & 0 & -z_{xP} & 0 & x_{xP} \\ 0 & 0 & 1 & y_{xP} & -x_{xP} & 0 \\ 1 & 0 & 0 & 0 & z_{xQ} & -y_{xQ} \\ 0 & 1 & 0 & -z_{xQ} & 0 & x_{xQ} \\ 0 & 0 & 1 & y_{xQ} & -x_{xQ} & 0 \\ 1 & 0 & 0 & 0 & z_{xK} & -y_{xK} \\ 0 & 1 & 0 & -z_{xK} & 0 & x_{xK} \\ 0 & 0 & 1 & y_{xK} & -x_{xK} & 0 \end{bmatrix} \begin{bmatrix} \delta_{xt}(x) \\ \delta_{yt}(x) \\ \delta_{zt}(x) \\ \varepsilon_{xt}(x) \\ \varepsilon_{yt}(x) \\ \varepsilon_{zt}(x) \end{bmatrix} = \begin{bmatrix} \Delta_{Pxt} \\ \Delta_{Pyt} \\ \Delta_{Pzt} \\ \Delta_{Qxt} \\ \Delta_{Qyt} \\ \Delta_{Qzt} \\ \Delta_{Kxt} \\ \Delta_{Kyt} \\ \Delta_{Kzt} \end{bmatrix} \tag{9}$$

where Δ_{ijt} (i=P, Q, or K, j=x, y, or z) denotes the volumetric error component at point i, in the direction of j-axis , at the tth step, and we give $\Delta_{ixt}=x'_{it}-x_{xi}-x_o-x$, $\Delta_{iyt}=y'_{it}-y_{xi}-y_o$, $\Delta_{izt}=z'_{it}-z_{xi}-z_o$ (i=P, Q, or K).

It can be proved that the rank of the coefficient matrix in Eq. 9 is full column rank as long as P, Q, and K do not lie on the same line. Hence, six equations can be properly selected from Eq. 12 to form a new system of equations which has a unique solution. Thus, in practical measuring procedures, the condition that the three selected points do not lie on the same line should be satisfied.

Number all the equations in Eq. 9 as ①~⑨, and divide them into three groups, i.e., the equations ①~③ are obtained by the error analysis of point P, the equations ④~⑥ are obtained by the error analysis of point Q, and the equations ⑦~⑨ are obtained by the error analysis of point K. In order to guarantee that the selected six equations have a unique solution, the following rules should be followed: at least one equation should be selected from each group, and the combinations ①②④⑤⑦⑧, ①③④⑥⑦⑨, and ②③⑤⑥⑧⑨ should not be used. In this paper, the combination ①②④⑥⑧⑨ is chosen to form a new system of equations

$$\begin{bmatrix} 1 & 0 & 0 & 0 & z_{xP} & -y_{xP} \\ 0 & 1 & 0 & -z_{xP} & 0 & x_{xP} \\ 1 & 0 & 0 & 0 & z_{xQ} & -y_{xQ} \\ 0 & 0 & 1 & y_{xQ} & -x_{xQ} & 0 \\ 0 & 1 & 0 & -z_{xK} & 0 & x_{xK} \\ 0 & 0 & 1 & y_{xK} & -x_{xK} & 0 \end{bmatrix} \begin{bmatrix} \delta_{xt}(x) \\ \delta_{yt}(x) \\ \delta_{zt}(x) \\ \varepsilon_{xt}(x) \\ \varepsilon_{yt}(x) \\ \varepsilon_{zt}(x) \end{bmatrix} = \begin{bmatrix} \Delta_{Pxt} \\ \Delta_{Pyt} \\ \Delta_{Qxt} \\ \Delta_{Qzt} \\ \Delta_{Kyt} \\ \Delta_{Kzt} \end{bmatrix} \tag{10}$$

and the solution is

$$\begin{aligned}
\delta_{xt}(x) &= \Delta_{Pxt} + \frac{M}{N}\left[y_{xP} - \frac{z_{xP}\left(y_{xQ}-y_{xP}\right)}{z_{xQ}-z_{xP}}\right] - \frac{z_{xP}\left(\Delta_{Qxt}-\Delta_{Pxt}\right)}{z_{xQ}-z_{xP}} \\
\delta_{yt}(x) &= \Delta_{Pyt} - \frac{M}{N}\left[x_{xP} - \frac{z_{xP}\left(x_{xP}-x_{xK}\right)}{z_{xP}-z_{xK}}\right] - \frac{z_{xP}\left(\Delta_{Pyt}-\Delta_{Kyt}\right)}{z_{xP}-z_{xK}} \\
\delta_{zt}(x) &= \Delta_{Qzt} + \frac{M}{N}\left[\frac{y_{xQ}\left(x_{xK}-x_{xP}\right)}{z_{xP}-z_{xK}} - \frac{x_{xQ}\left(y_{xP}-y_{xQ}\right)}{z_{xQ}-z_{xP}}\right] - \frac{y_{xQ}\left(\Delta_{Kyt}-\Delta_{Pyt}\right)}{z_{xP}-z_{xK}} + \frac{x_{xQ}\left(\Delta_{Qxt}-\Delta_{Pxt}\right)}{z_{xQ}-z_{xP}} \\
\varepsilon_{xt}(x) &= \frac{\Delta_{Kyt}-\Delta_{Pyt}}{z_{xP}-z_{xK}} + \frac{x_{xP}-x_{xK}}{z_{xP}-z_{xK}} \cdot \frac{M}{N} \\
\varepsilon_{yt}(x) &= \frac{\Delta_{Qxt}-\Delta_{Pxt}}{z_{xQ}-z_{xP}} + \frac{y_{xQ}-y_{xP}}{z_{xQ}-z_{xP}} \cdot \frac{M}{N} \\
\varepsilon_{zt}(x) &= \frac{M}{N}
\end{aligned} \tag{11}$$

where

$$\begin{aligned}
M &= \left(\Delta_{Qxt}-\Delta_{Pxt}\right)\left(x_{xK}-x_{xQ}\right)\left(z_{xP}-z_{xK}\right) + \\
&\quad \left[\left(\Delta_{Pyt}-\Delta_{Kyt}\right)\left(y_{xK}-y_{xQ}\right) + \left(\Delta_{Kzt}-\Delta_{Qzt}\right)\left(z_{xP}-z_{xK}\right)\right]\left(z_{xQ}-z_{xP}\right) \\
N &= \left(x_{xK}-x_{xQ}\right)\left(y_{xP}-y_{xQ}\right)\left(z_{xP}-z_{xK}\right) - \left(x_{xK}-x_{xP}\right)\left(y_{xK}-y_{xQ}\right)\left(z_{xQ}-z_{xP}\right)
\end{aligned}$$

In Eq. 11, N is a denominator. Thus, in practical measuring procedures, besides making sure that the three selected points do not lie on the same line, the positions of the three under-test points should be reasonably arranged to guarantee that N is not zero. The simplest way is to make the z-coordinates of the three points differ with each other. Considering the measurement for the x-slide, y-slide, and z-slide, as well as the different way for

extracting equations from Eq. 9, practical measurement should follow the following rules: the *i*-coordinates (*i*=*x*, *y*, or *z*) of these three points are not equal to each other.

4.1.2 Geometric error measurement for the rotary axis

The geometric error components measurement for the rotary axis is similar to that for the linear axis. We take the *C*-axis as an example to demonstrate the method for measuring the geometric error components of rotary axis [35]. As shown in Fig. 4, three noncollinear points, *P*, *Q*, and *K* are selected on the stage, and the coordinates of *P*, *Q*, and *K* are (x_{CP}, y_{CP}, z_{CP}), (x_{CQ}, y_{CQ}, z_{CQ}), and (x_{CK}, y_{CK}, z_{CK}), respectively. *oxyz* is the reference coordinate frame and $o_C x_C y_C z_C$ is the *C*-axis coordinate frame.

The homogeneous coordinates of o_C is $[x_o, y_o, z_o, 1]^T$ in the reference coordinate frame at the beginning. At time *t*, the angular displacement of *C*-axis is θ. If there are no errors while the *C*-axis is rotating, the homogeneous coordinates of o_C are

$$\begin{bmatrix} x_{ot} \\ y_{ot} \\ z_{ot} \\ 1 \end{bmatrix} = \begin{bmatrix} 1 & 0 & 0 & 0 \\ 0 & 1 & 0 & 0 \\ 0 & 0 & 1 & 0 \\ 0 & 0 & 0 & 1 \end{bmatrix} \begin{bmatrix} x_o \\ y_o \\ z_o \\ 1 \end{bmatrix} = \begin{bmatrix} x_o \\ y_o \\ z_o \\ 1 \end{bmatrix} \tag{12}$$

The homogeneous coordinates of point *P* are

$$\begin{bmatrix} x_{Pt} \\ y_{Pt} \\ z_{Pt} \\ 1 \end{bmatrix} = \begin{bmatrix} \cos\theta & -\sin\theta & 0 & x_{ot} \\ \sin\theta & \cos\theta & 0 & y_{ot} \\ 0 & 0 & 1 & z_{ot} \\ 0 & 0 & 0 & 1 \end{bmatrix} \begin{bmatrix} x_{CP} \\ y_{CP} \\ z_{CP} \\ 1 \end{bmatrix} \tag{13}$$

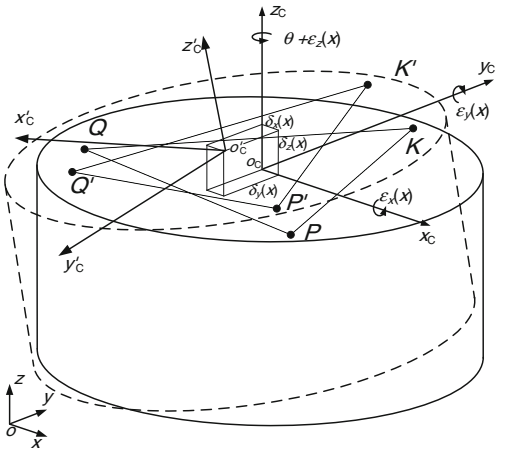

Fig. 4 Geometric error components measurement of *C*-axis

The actual coordinates of *P* is (x'_{Pt}, y'_{Pt}, z'_{Pt}) which can be collected by a laser tracker. Assume that the three volumetric error components at point *P* are Δ_{Pxt}, Δ_{Pyt}, and Δ_{Pzt}, so we have

$$\begin{bmatrix} \Delta_{Pxt} \\ \Delta_{Pyt} \\ \Delta_{Pzt} \\ 0 \end{bmatrix} = \begin{bmatrix} x'_{Pt} \\ y'_{Pt} \\ z'_{Pt} \\ 1 \end{bmatrix} - \begin{bmatrix} x_{Pt} \\ y_{Pt} \\ z_{Pt} \\ 1 \end{bmatrix} \tag{14}$$

Substitute Eqs. 12, 13, and 14 into Eq. 4 and eliminate the volumetric error components, we get

$$\begin{cases} x'_{Pt} - x_{CP}\cos\theta + y_{CP}\sin\theta - x_o = -\varepsilon_{zt}(\theta)(x_{CP}\sin\theta + y_{CP}\cos\theta) + \varepsilon_{yt}(\theta) z_{CP} + \delta_{xt}(\theta) \\ y'_{Pt} - x_{CP}\sin\theta - y_{CP}\cos\theta - y_o = \varepsilon_{zt}(\theta)(x_{CP}\cos\theta - y_{CP}\sin\theta) - \varepsilon_{xt}(\theta) z_{CP} + \delta_{yt}(\theta) \\ z'_{Pt} - z_{CP} - z_o = \left[-\varepsilon_{yt}(\theta)\cos\theta + \varepsilon_{xt}(\theta)\sin\theta\right] x_{CP} + \left[\varepsilon_{yt}(\theta)\sin\theta + \varepsilon_{xt}(\theta)\cos\theta\right] y_{CP} + \delta_{zt}(\theta) \end{cases} \tag{15}$$

The same procedure is performed on points *Q* and *K*, and rewriting all the nine equations in matrix form, we get

$$\begin{bmatrix} 1 & 0 & 0 & 0 & z_{CP} & -\hat{y}_{CP} \\ 0 & 1 & 0 & -z_{CP} & 0 & \hat{x}_{CP} \\ 0 & 0 & 1 & \hat{y}_{CP} & -\hat{x}_{CP} & 0 \\ 1 & 0 & 0 & 0 & z_{CQ} & -\hat{y}_{CQ} \\ 0 & 1 & 0 & -z_{CQ} & 0 & \hat{x}_{CQ} \\ 0 & 0 & 1 & \hat{y}_{CQ} & -\hat{x}_{CQ} & 0 \\ 1 & 0 & 0 & 0 & z_{CK} & -\hat{y}_{CK} \\ 0 & 1 & 0 & -z_{CK} & 0 & \hat{x}_{CK} \\ 0 & 0 & 1 & \hat{y}_{CK} & -\hat{x}_{CK} & 0 \end{bmatrix} \begin{bmatrix} \delta_{xt}(\theta) \\ \delta_{yt}(\theta) \\ \delta_{zt}(\theta) \\ \varepsilon_{xt}(\theta) \\ \varepsilon_{yt}(\theta) \\ \varepsilon_{zt}(\theta) \end{bmatrix} = \begin{bmatrix} \Delta_{Pxt} \\ \Delta_{Pyt} \\ \Delta_{Pzt} \\ \Delta_{Qxt} \\ \Delta_{Qyt} \\ \Delta_{Qzt} \\ \Delta_{Kxt} \\ \Delta_{Kyt} \\ \Delta_{Kzt} \end{bmatrix} \tag{16}$$

where Δ_{ijt} (*i*=*P*, *Q*, or *K*, *j*=*x*, *y*, or *z*) denotes the volumetric error component at point *i*, in the direction of *j*-axis, at the *t*th step, and we give $\Delta_{ixt} = x'_{it} - \hat{x}_{Ci} - x_o$, $\Delta_{iyt} = y'_{it} - \hat{y}_{Ci} - y_o$, $\Delta_{izt} = z'_{it} - \hat{z}_{Ci} - z_o$, $\hat{x}_{Ci} = x_{Ci}\cos\theta - y_{Ci}\sin\theta$, $\hat{y}_{Ci} = y_{Ci}\cos\theta + x_{Ci}\sin\theta$, (*i*=*P*, *Q*, or *K*).

The selected points *P*, *Q*, and *K* should not be located on the same line, which can guarantee that a set of six equations selected from Eq. 16 has a unique solution. Similar to the analysis in the previous section, a new system of equations is established by extracting the six equations from Eq. 16

$$\begin{bmatrix} 1 & 0 & 0 & 0 & z_{CP} & -\hat{y}_{CP} \\ 0 & 1 & 0 & -z_{CP} & 0 & \hat{x}_{CP} \\ 1 & 0 & 0 & 0 & z_{CQ} & -\hat{y}_{CQ} \\ 0 & 0 & 1 & \hat{y}_{CQ} & -\hat{x}_{CQ} & 0 \\ 0 & 1 & 0 & -z_{CK} & 0 & \hat{x}_{CK} \\ 0 & 0 & 1 & \hat{y}_{CK} & -\hat{x}_{CK} & 0 \end{bmatrix} \begin{bmatrix} \delta_{xt}(\theta) \\ \delta_{yt}(\theta) \\ \delta_{zt}(\theta) \\ \varepsilon_{xt}(\theta) \\ \varepsilon_{yt}(\theta) \\ \varepsilon_{zt}(\theta) \end{bmatrix} = \begin{bmatrix} \Delta_{Pxt} \\ \Delta_{Pyt} \\ \Delta_{Qxt} \\ \Delta_{Qzt} \\ \Delta_{Kyt} \\ \Delta_{Kzt} \end{bmatrix} \tag{17}$$

Solving Eq. 17, we obtain

$$\delta_{xt}(\theta) = \Delta_{Pxt} + \frac{M}{N}\left[\widehat{y}_{CP} - \frac{z_{CP}(\widehat{y}_{CQ} - \widehat{y}_{CP})}{z_{CQ} - z_{CP}}\right] - \frac{z_{CP}(\Delta_{Qxt} - \Delta_{Pxt})}{z_{CQ} - z_{CP}}$$

$$\delta_{yt}(\theta) = \Delta_{Pyt} - \frac{M}{N}\left[\widehat{x}_{CP} - \frac{z_{CP}\left(\widehat{x}_{CP} - \widehat{x}_{CK}\right)}{z_{CP} - z_{CK}}\right] - \frac{z_{CP}(\Delta_{Pyt} - \Delta_{Kyt})}{z_{CP} - z_{CK}}$$

$$\delta_{zt}(\theta) = \Delta_{Qzt} + \frac{M}{N}\left[\frac{\widehat{y}_{CQ}\left(\widehat{x}_{CK} - \widehat{x}_{CP}\right)}{z_{CP} - z_{CK}} - \frac{\widehat{x}_{CQ}\left(\widehat{y}_{CP} - \widehat{y}_{CQ}\right)}{z_{CQ} - z_{CP}}\right] - \frac{\widehat{y}_{CQ}(\Delta_{Kyt} - \Delta_{Pyt})}{z_{CP} - z_{CK}} + \frac{\widehat{x}_{CQ}(\Delta_{Qxt} - \Delta_{Pxt})}{z_{CQ} - z_{CP}} \tag{18}$$

$$\varepsilon_{xt}(\theta) = \frac{\Delta_{Kyt} - \Delta_{Pyt}}{z_{CP} - z_{CK}} + \frac{\widehat{x}_{CP} - \widehat{x}_{CK}}{z_{CP} - z_{CK}} \cdot \frac{M}{N}$$

$$\varepsilon_{yt}(\theta) = \frac{\Delta_{Qxt} - \Delta_{Pxt}}{z_{CQ} - z_{CP}} + \frac{\widehat{y}_{CQ} - \widehat{y}_{CP}}{z_{CQ} - z_{CP}} \cdot \frac{M}{N}$$

$$\varepsilon_{zt}(\theta) = \frac{M}{N}$$

where

$$M = (\Delta_{Qxt} - \Delta_{Pxt})\left(\widehat{x}_{CK} - \widehat{x}_{CQ}\right)(z_{CP} - z_{CK}) + \left[(\Delta_{Pyt} - \Delta_{Kyt})\left(\widehat{y}_{CK} - \widehat{y}_{CQ}\right) + (\Delta_{Kzt} - \Delta_{Qzt})(z_{CP} - z_{CK})\right](z_{CQ} - z_{CP})$$

$$N = \left(\widehat{x}_{CK} - \widehat{x}_{CQ}\right)\left(\widehat{y}_{CP} - \widehat{y}_{CQ}\right)(z_{CP} - z_{CK}) - \left(\widehat{x}_{CK} - \widehat{x}_{CP}\right)\left(\widehat{y}_{CK} - \widehat{y}_{CQ}\right)(z_{CQ} - z_{CP})$$

In Eq. 18, N is a denominator. Thus, in practical measuring procedure, the positions of the points P, Q, and K should be reasonably arranged to guarantee that N is not zero. Firstly, the z-coordinates of P, K, and Q should not be same to each other. Secondly, the angular step of the rotary axis should be reasonably selected to guarantee that N is not zero at each step.

4.1.3 General method for identifying the geometric errors of a single axis

The Eqs. 9, 10, and 11 are found similar to Eqs. 16, 10, and 11, respectively. So the proposed method can be considered as a general method for identifying the geometric errors of a single axis, including the linear and rotary axes.

A single axis, whether it is linear axis or rotary axis, can be considered as a generalized axis. The three generalized coordinates are $\widehat{x}$, $\widehat{y}$ and $\widehat{z}$, which are defined as follow.

When testing the linear x-axis or rotary x-axis (A-axis), we define

$$\widehat{x} = x, \widehat{y} = y\ \cos\ \alpha - z\ \sin\ \alpha, \widehat{z} = z\ \cos\ \alpha + y\ \sin\ \alpha \tag{19a}$$

When testing the linear y-axis or rotary y-axis (B-axis), we define

$$\widehat{y} = y, \widehat{z} = z\ \cos\ \beta - x\ \sin\ \beta, \widehat{x} = x\ \cos\ \beta + z\ \sin\ \beta \tag{19b}$$

When testing the linear z-axis or rotary z-axis (C-axis), we define

$$\widehat{z} = z, \widehat{x} = x\ \cos\ \theta - y\ \sin\ \theta, \widehat{y} = y\ \cos\ \theta + x\ \sin\ \theta \tag{19c}$$

Subsequently, the error model in Eq. 20 can be collectively considered as a generalized expression of Eqs. 1 and 3, i.e., it is a generalized error model of an arbitrary single axis.

$$\begin{bmatrix} \Delta_x(i) \\ \Delta_y(i) \\ \Delta_z(i) \\ 0 \end{bmatrix} = \begin{bmatrix} 0 & -\varepsilon_z(i) & \varepsilon_y(i) & \delta_x(i) \\ \varepsilon_z(i) & 0 & -\varepsilon_x(i) & \delta_y(i) \\ -\varepsilon_y(i) & \varepsilon_x(i) & 0 & \delta_z(i) \\ 0 & 0 & 0 & 0 \end{bmatrix} \begin{bmatrix} \widehat{x}_t \\ \widehat{y}_t \\ \widehat{z}_t \\ 1 \end{bmatrix} \tag{20}$$

As a result, when testing a generalized single i-axis (i=$\widehat{x}$, $\widehat{y}$ or $\widehat{z}$), nine equations shown in Eq. 21 can be established.

$$\begin{bmatrix} \boldsymbol{I} & \boldsymbol{M}_P \\ \boldsymbol{I} & \boldsymbol{M}_Q \\ \boldsymbol{I} & \boldsymbol{M}_K \end{bmatrix} \cdot \boldsymbol{E}_{it} = \begin{bmatrix} \boldsymbol{\Delta}_{Pt} \\ \boldsymbol{\Delta}_{Qt} \\ \boldsymbol{\Delta}_{Kt} \end{bmatrix} \tag{21}$$

where

$$\boldsymbol{M}_j = \begin{bmatrix} 0 & \widehat{z}_j & -\widehat{y}_j \\ -\widehat{z}_j & 0 & \widehat{x}_j \\ \widehat{y}_j & -\widehat{x}_j & 0 \end{bmatrix} \quad j = P, Q \text{ or } K$$

and where $\boldsymbol{I}$ is the identity matrix; $\boldsymbol{E}_{it}=[\delta_{xt},\ \delta_{yt},\ \delta_{zt},\ \varepsilon_{xt},\ \varepsilon_{yt},\ \varepsilon_{zt}]^{\mathrm{T}}$; $\boldsymbol{\Delta}_{jt}=[\Delta_{jxt},\ \Delta_{jyt},\ \Delta_{jzt}]$ denotes the three volumetric error components at point j, at the tth step; $\widehat{x}_j$, $\widehat{y}_j$, and $\widehat{z}_j$ are the generalized coordinates.

Six equations can be properly selected from Eq. 21, and the six geometric error components shown in Eq. 22 can be obtained by solving these six equations.

$$\begin{aligned}
\delta_{xt} &= \Delta_{Pxt} + \frac{M}{N}\left[\widehat{y}_P - \frac{\widehat{z}_P\left(\widehat{y}_Q - \widehat{y}_P\right)}{\widehat{z}_Q - \widehat{z}_P}\right] - \frac{\widehat{z}_P\left(\Delta_{Qxt} - \Delta_{Pxt}\right)}{\widehat{z}_Q - \widehat{z}_P} \\
\delta_{yt} &= \Delta_{Pyt} - \frac{M}{N}\left[\widehat{x}_P - \frac{\widehat{z}_P\left(\widehat{x}_P - \widehat{x}_K\right)}{\widehat{z}_P - \widehat{z}_K}\right] - \frac{\widehat{z}_P\left(\Delta_{Pyt} - \Delta_{Kyt}\right)}{\widehat{z}_P - \widehat{z}_K} \\
\delta_{zt} &= \Delta_{Qzt} + \frac{M}{N}\left[\frac{\widehat{y}_Q\left(\widehat{x}_K - \widehat{x}_P\right)}{\widehat{z}_P - \widehat{z}_K} - \frac{\widehat{x}_Q\left(\widehat{y}_P - \widehat{y}_Q\right)}{\widehat{z}_Q - \widehat{z}_P}\right] - \frac{\widehat{y}_Q\left(\Delta_{Kyt} - \Delta_{Pyt}\right)}{\widehat{z}_P - \widehat{z}_K} + \frac{\widehat{x}_Q\left(\Delta_{Qxt} - \Delta_{Pxt}\right)}{\widehat{z}_Q - \widehat{z}_P} \\
\varepsilon_{xt} &= \frac{\Delta_{Kyt} - \Delta_{Pyt}}{\widehat{z}_P - \widehat{z}_K} + \frac{\widehat{x}_P - \widehat{x}_K}{\widehat{z}_P - \widehat{z}_K} \cdot \frac{M}{N} \\
\varepsilon_{yt} &= \frac{\Delta_{Qxt} - \Delta_{Pxt}}{\widehat{z}_Q - \widehat{z}_P} + \frac{\widehat{y}_Q - \widehat{y}_P}{\widehat{z}_Q - \widehat{z}_P} \cdot \frac{M}{N} \\
\varepsilon_{zt} &= \frac{M}{N}
\end{aligned} \tag{22}$$

where

$$\begin{aligned}
M &= \left(\Delta_{Qxt} - \Delta_{Pxt}\right)\left(\widehat{x}_K - \widehat{x}_Q\right)\left(\widehat{z}_P - \widehat{z}_K\right) + \left[\left(\Delta_{Pyt} - \Delta_{Kyt}\right)\left(\widehat{y}_K - \widehat{y}_Q\right) + \left(\Delta_{Kzt} - \Delta_{Qzt}\right)\left(\widehat{z}_P - \widehat{z}_K\right)\right]\left(\widehat{z}_Q - \widehat{z}_P\right) \\
N &= \left(\widehat{x}_K - \widehat{x}_Q\right)\left(\widehat{y}_P - \widehat{y}_Q\right)\left(\widehat{z}_P - \widehat{z}_K\right) - \left(\widehat{x}_K - \widehat{x}_P\right)\left(\widehat{y}_K - \widehat{y}_Q\right)\left(\widehat{z}_Q - \widehat{z}_P\right)
\end{aligned}$$

4.2 Determination of the location errors of each axis

4.2.1 Establishing the reference coordinate frame

To determine the location errors of each axis, a reference coordinate frame should firstly be established.

As shown in Fig. 5, the real trace of the origin of the *x*-slide coordinate frame is a space curve. Linear curve fitting is applied to obtain the average line of the *x*-slide which passes through the origin. This average line is considered as the *x*-axis of the reference coordinate frame. The real trace of the origin of the *y*-slide is also a space curve. Similarly, linear curve fitting is applied to obtain the average line of the *y*-slide which also passes through the origin. The average lines of the *x*-slide and *y*-slide form a plane named the *x*-*y* plane of the reference coordinate frame, and then a straight line which passes through the origin and is perpendicular to the *x*-axis is created within the *x*–*y* plane. This straight line is regarded as the *y*-axis of the reference coordinate frame. Finally, the third straight line which passes through the origin and is perpendicular to the *x*–*y* plane is created, and it is considered to be the *z*-axis of the reference coordinate frame. The directions of each axis of the reference coordinate frame must follow the right-hand rule. The reference coordinate frame is thus established.

4.2.2 Determination of the squareness error

As shown in Fig. 5, S_{xy} is the squareness error between the *x*-slide and the *y*-slide, and it can be represented by the rotation angle of the *y*-slide about the reference *z*-axis. S_{xz} is the squareness error between *z*-slide and the *x*-slide, and S_{yz} is the squareness error between *z*-slide and *y*-slide, respectively. θ_{xz} and θ_{yz} are the angles between the *z*-axis of reference coordinate frame and the projection of the average line of z-slide on the *x*–*z* plane and the *y*–*z* plane,

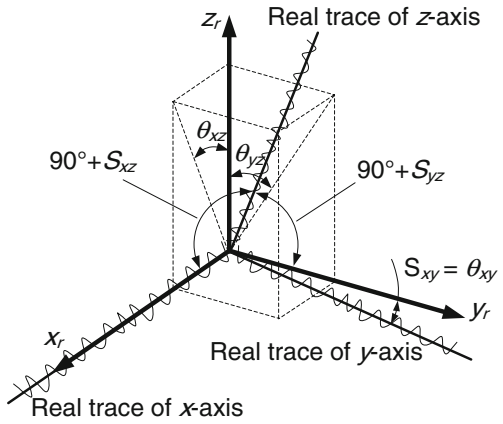

Fig. 5 Three squareness errors between three linear axis

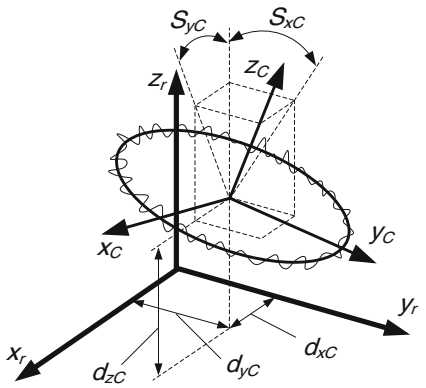

Fig. 6 Five location parameters of rotary axis

respectively. In accordance with the small error hypothesis, θ_{xz} and θ_{yz} are approximately equal to S_{xz} and S_{yz}. The sign symbols of these three squareness errors obey the right-hand rule.

Obviously, squareness errors can be determined by the locations of the average lines of the three slides which are described by linear equations. Since the coordinate sequence of the origin of each coordinate frame can be measured by a laser tracker, the linear fitting method can be applied to obtain the mathematical expression of the average line of each axis. If the mathematical expression of the average lines of the x-slide, the y-slide, and the z-slide are

$$\frac{x}{m_x}=\frac{y}{n_x}=\frac{z}{1},\quad \frac{x}{m_y}=\frac{y}{n_y}=\frac{z}{1},\quad \frac{x}{m_z}=\frac{y}{n_z}=\frac{z}{1}$$

Then the three squareness errors can be derive from the three normal vectors of the three average lines, i.e., (m_x, n_x, 1), (m_y, n_y, 1), and (m_z, n_z, 1).

$$\begin{aligned}\theta_{xy} &= 90-\arccos\frac{m_xm_y+n_xn_y+1}{\sqrt{m_x^2+n_x^2+1}\sqrt{m_y^2+n_y^2+1}}\\ \theta_{xz} &= \arctan\frac{\cos\alpha}{\sqrt{1-\cos^2\alpha-\cos^2\beta}}\\ \theta_{yz} &= \arctan\frac{\cos\beta}{\sqrt{1-\cos^2\alpha-\cos^2\beta}}\end{aligned}\tag{23}$$

where

$$\cos\alpha=\frac{m_xm_z+n_xn_z+1}{\sqrt{m_x^2+n_x^2+1}\sqrt{m_z^2+n_z^2+1}},\quad \cos\beta=\frac{m_ym_z+n_yn_z+1}{\sqrt{m_y^2+n_y^2+1}\sqrt{m_z^2+n_z^2+1}}$$

4.2.3 Determination of location error components of rotary axis

Taking the C-axis as the example, how to determine the location errors of rotary axis is presented in this section. As shown in Fig. 6, there are totally five location parameters, i.e., d_{xC}, d_{yC}, and d_{zC} are the three offset, and S_{xC} and S_{yC} are the two angular errors. These location parameters can be determined by the location of the average circle which is described mathematically. Since the coordinate sequence of the origin of the C-axis coordinate frame can be grabbed by a laser tracker, curve fitting can be used to obtain the mathematical expression of the average circle. If the origin of the C-axis coordinate frame (the center point of the average circle) is located at (x_{0C}, y_{0C}, z_{0C}) and the normal vector to the average circle plane is $\boldsymbol{V}$ (A, B, C), we can show that d_{xC}=x_{0C}, d_{yC}=y_{0C}, and d_{zC}=z_{0C}, and that S_{xC}=arctan(B/C) and S_{yC}=arctan(A/C), respectively.

5 Error measurement experiments

To demonstrate the practicability of the proposed method, several experiments were conducted by using a commercial FARO laser tracker based on the sequential multilateration in which the performance is demonstrated in Section 3. Due to the fact that there were no machine tools with one or more rotary axis available, we had to conduct two experiments to verify the proposed methods discussed in this paper. The first one is identifying all the geometric error components of a three-axis machine tool; the other one is measuring the six geometric error components of a single rotary stage.

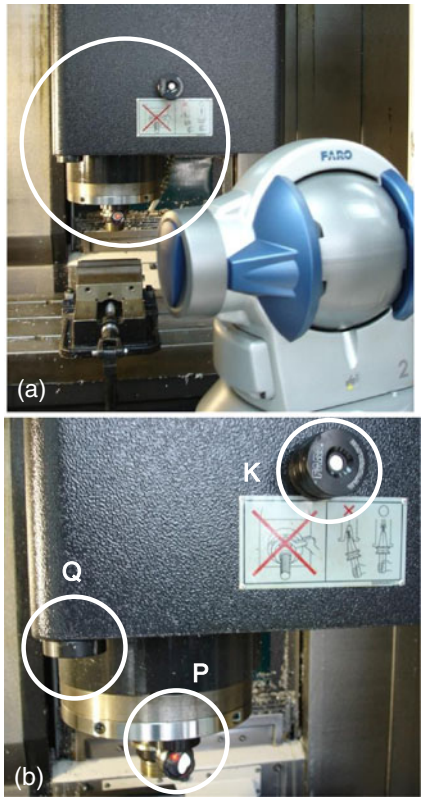

Fig. 7 The setup used in the experiments. **a** The setup; **b** the arrangement of three points

5.1 Error measurements for three-axis machine tools

As shown in Fig. 7, an experiment is conducted to measure the 21 geometric error components of a three-axis machine tool of type FXYZ. The strokes of x-axis, y-axis, and z-axis are 440, 400, and 400 mm, respectively.

The measuring steps are:

1. Three targets P, K, and Q are fixed on the spindle assembly. Their t-coordinates (t is x, y, and z, respectively) are observably not the same.
2. The spindle assembly moves in steps of 20 mm along each axis, meanwhile the coordinate sequences of the three selected points P, K, and Q can be measured by the sequential multilateration method.
3. By establishing the reference coordinate frame following the rule stated in Section 4.2.1, the three squareness errors can be determined by using Eq. 23.
4. These measured coordinate sequences are transformed into new coordinate sequences under the reference coordinate frame. In the experiments, the coordinates of the three points in the reference coordinate frame are P_0 (16.338, 452.716, 122.416), Q_0 (157.086, 332.593, 324.879), and K_0 (248.925, 603.0552, 412.4483), respectively, while the machine tool is in the home position.
5. Substitute these new coordinate sequences into Eq. 11 to obtain the six geometric error components of each axis.

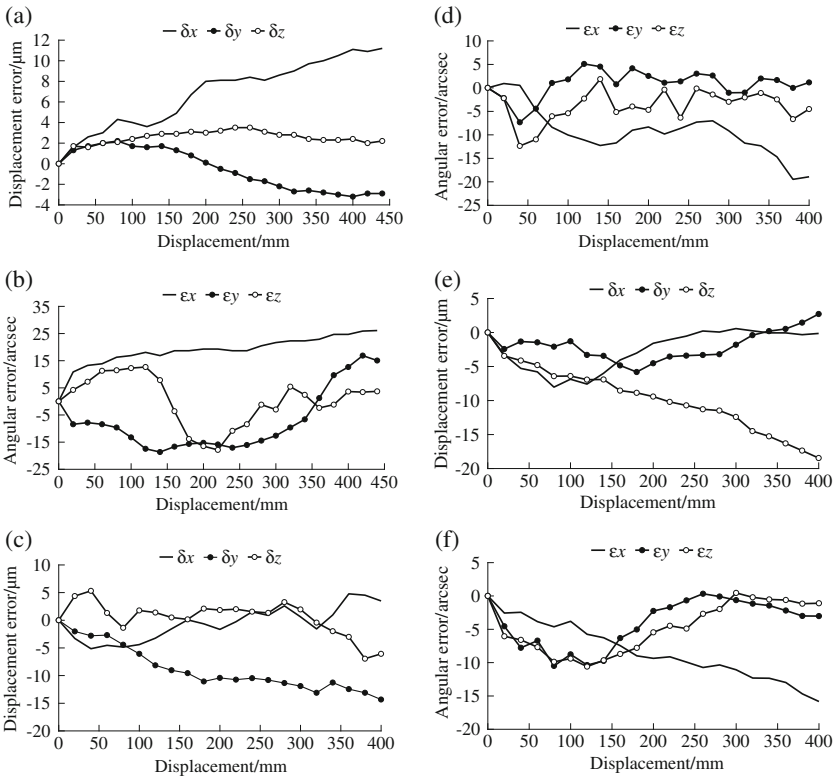

Fig. 8 The six geometric error components of each axis. **a** Three displacement errors of the x-axis; **b** three angular errors of the x-axis; **c** three displacement errors of the y-axis; **d** three angular errors of the y-axis; **e** three displacement errors of the z-axis; **f** three angular errors of the z-axis

The measurement mentioned above is repeated 10 times and the mean values of each geometric error components can be obtained. So far, all the geometric error components have been measured. The experimental results of the three squareness errors are that S_{xy} is −22.925 arcsec, S_{xz} is −27.377 arcsec, and S_{yz} is 19.614 arcsec, the results of the other 18 geometric error components are shown in Fig. 8.

The laser interferometer is an acknowledged high-accuracy device for machine tool calibration, so it is used to conduct a comparative experiment to verify the effectiveness of the proposed method. The setup is shown in Fig. 9. Firstly, software compensation is applied to compensate the volumetric errors of this three-axis machine tool [36], and then a target point fixed on the spindle assembly moves along the *x*-axis, the *y*-axis, and the *z*-axis, respectively. Meanwhile, the positioning errors of this moving point are measured by using a laser interferometer, without compensation and with compensation respectively. The coordinates of this measured point *T* are (175.6, 497.5, 312.1) when the machine tool is in the home position. The sample interval is 10 mm. The results of comparative experiment are shown in Fig. 10. Obviously, the positioning errors of point *T* along three axes are significantly reduced. The maximum errors along the *x*-axis are reduced from 16.69 to 5.11 μm; the maximum errors along the *y*-axis are reduced from −17.52 to −4.47 μm; the maximum errors along the *z*-axis are reduced from −18.38 to −4.67 μm. In conclusion, error compensation can enhance the accuracy, and the proposed method for the geometric error component measurements of three-axis machine tools is effective.

To further validate the proposed method, other comparative experiments are conducted to measure the pitch errors and yaw errors of the three axis by using the methods presented in the literature [8]. The method for measuring the pitch error and yaw error of *x*-axis is shown in Fig. 11. Specifically, the *x*-axis moves step by step with a step size of

Fig. 9 Measuring positioning errors by using laser interferometer

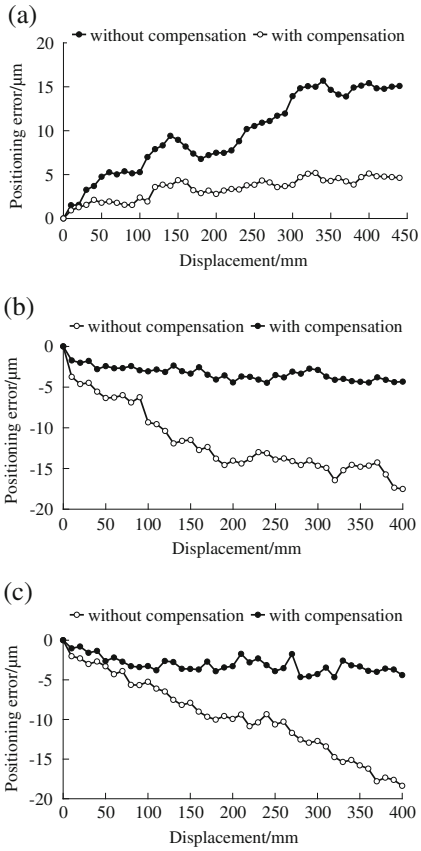

Fig. 10 Results of comparison experiments. **a** The positioning error along *x*-axis; **b** the positioning error along *y*-axis; **c** the positioning error along *z*-axis

20 mm, and at each step, the displacements along the three lines L1 (y=0, z=0), L2 (y=y_1, z=0), and L3 (y=0, z=z_1) are measured by a laser interferometer. Then we give

$$\varepsilon_{yi}(x) = [\Delta L_3(x_i, 0, z_1) - \Delta L_1(x_i, 0, 0)]/z_1$$
$$\varepsilon_{zi}(x) = [\Delta L_2(x_i, y_1, 0) - \Delta L_1(x_i, 0, 0)]/y_1$$

where the $\varepsilon_{yi}(x)$ and $\varepsilon_{zi}(x)$ are the pitch error and yaw error at the *i*th step, the $\Delta L_1(x_i, 0, 0)$, $\Delta L_2(x_i, y_1, 0)$, and $\Delta L_3(x_i, 0, z_1)$ are the displacement errors along lines L1, L2, and L3, at the *i*th step, respectively.

The method for measuring the pitch errors and yaw errors of *y*-axis and *z*-axis are similar to the method mentioned above. As shown in Fig. 12, the errors measured by laser tracker (LT) are compared to the errors measured by the laser interferometer (LI). For the pitch errors and yaw errors of *x*-axis, the maximum deviation is 4.07″ and 3.12″, respectively; for the pitch errors and yaw errors of *y*-axis, the maximum deviation is 2.74″ and 2.95″, respectively; for the pitch errors and yaw errors of *z*-axis, the maximum deviation is 1.81″ and 1.94″, respectively. The effectiveness of the proposed method for measuring the geometric error component of the three-axis machine tools is accordingly verified.

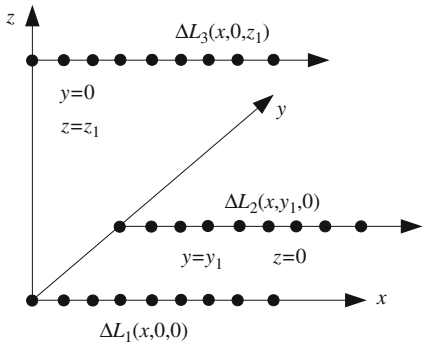

Fig. 11 The method for measuring pitch error and yaw error by using laser interferometer

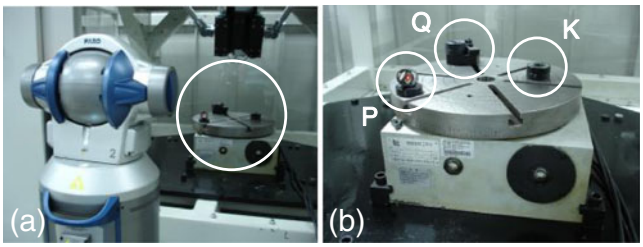

Fig. 13 The setup of the geometric error components measurement for the rotary axis. **a** The setup; **b** the arrangement of the three points

5.2 Error measurements for the rotary axis

A rotary stage is tested as shown in Fig. 13. The measuring steps are:

1. Three targets *P*, *K*, and *Q* are fixed on the rotary stage with initial coordinates P'_0 (1005.6648, −140.3849, −222.6797), Q'_0 (1240.2676, −187.6319, −183.0147), and K'_0 (1136.3720, −386.5078, −207.4099) respectively in the coordinate frame of laser-tracker measuring system.
2. The stage rotates step by step with a step size of 20°. Meanwhile, the coordinate sequences of these three points can be detected by the laser tracker.
3. Circular curve fitting is applied to establish the coordinate frame. The center of the circle is (111.447, −257.739, −221.528) in the coordinate frame of the laser-tracker measuring system. The location errors can then be determined, i.e., the offsets are d_{xC}=111.447 mm, d_{yC}=−257.739 mm, and d_{zC}=−221.528 mm, S_{xC}=39.082 arcsec and S_{yC}=−17.341 arcsec, respectively. The initial coordinates of *P*, *K*, and *Q* are P_0 (−105.8046, 135.3414, 0), Q_0 (128.8513, 87.8158, 39.9797), K_0 (24.9026, −110.8575, 15.2662) in the rotary stage coordinate frame.
4. Then check whether *N* in Eq. 18 is equal to zero or not at each step; if so, the step size or the position of the three points should be changed, and return to step 1 until *N* is not zero. In this experiment, a step size of 20° can guarantee that *N* is not zero at each step.

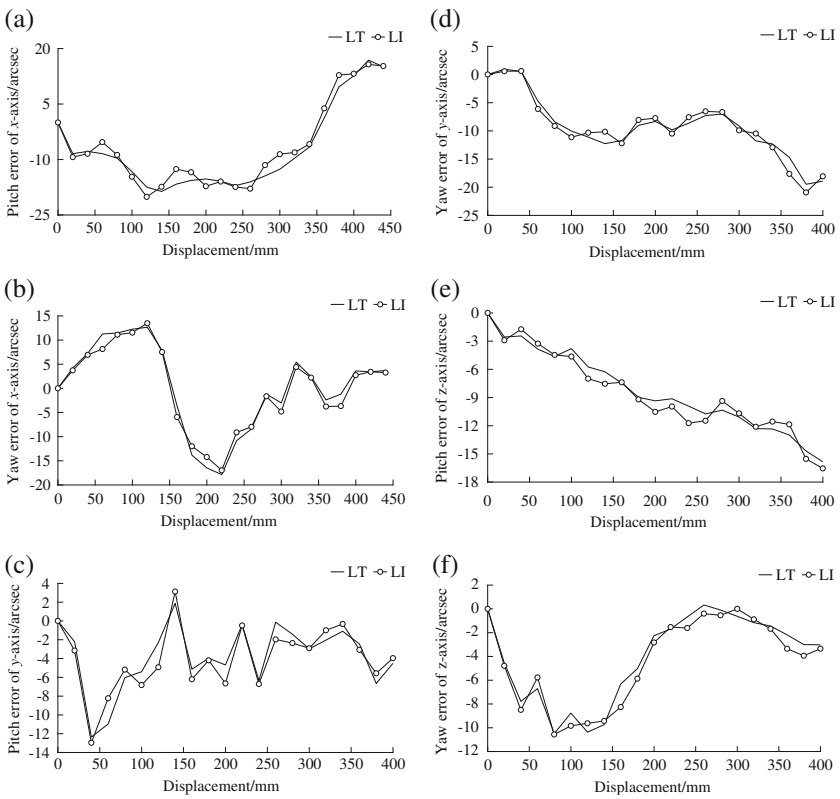

Fig. 12 **a**–**f** The errors obtained by laser tracker (*LT*) and laser interferometer (*LI*)

5. All the six geometric error components can be determined by making use of these data and the Eq. 18.

The measurement procedure is repeated 10 times. The results of the measurements are shown in Fig. 14.

In order to validate this method for geometric error component measurement of the rotary stage, comparative experiments are conducted. Restricted by limited equipment and instruments, we could not measure each one of the six geometric error components of the rotary stage by other methods. In this paper, QC10, a double ballbar, is applied to indirectly evaluate the volumetric error vectors of target points. As illustrated in Fig. 15a, the pivot assembly is fixed on the rotary stage and the measuring ball is attached to the top of the pivot assembly, A is the center of the measuring ball with coordinates (x_A, y_A, z_A) in the rotary stage coordinate frame; the center ball is attached to a point O which is located right above the center of the stage. The rotary stage rotates in steps of 20°, and the length change of the ballbar, ΔL, is tested by DBB at each step. The ΔL between the center ball and the measuring ball is mainly caused by the error vector $\Delta_{\mathbf{E}}$ $[\Delta_{Ax}, \Delta_{Ay}, \Delta_{Az}]^T$. Thus, as shown in Fig. 15b,

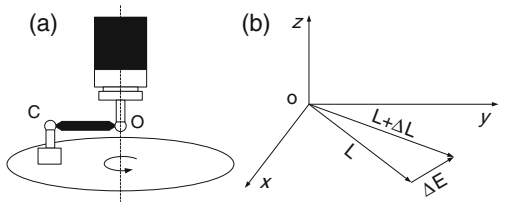

Fig. 15 Testing the volumetric error vector using DBB. **a** The principle; **b** relationship between the error vector and the length change of DBB

$(\mathbf{L}+\Delta\mathbf{L})=\mathbf{L}+\Delta_{\mathbf{E}}$ is given. By ignoring the high order infinitely small quantity, the following equation can be obtained [37]

$$\Delta L = \frac{1}{L}\left(x_A\Delta_{Ax} + y_A\Delta_{Ay} + z_A\Delta_{Az}\right) \tag{24}$$

The (Δ_{Ax}, Δ_{Ay}, Δ_{Az}) can be obtained by using Eq. 4, and the six geometric error components in Eq. 4 have been measured. Hence, the ΔL can be obtained.

We can indirectly verify the proposed method by comparing the ΔLs obtained by vector operation with the ΔLs tested

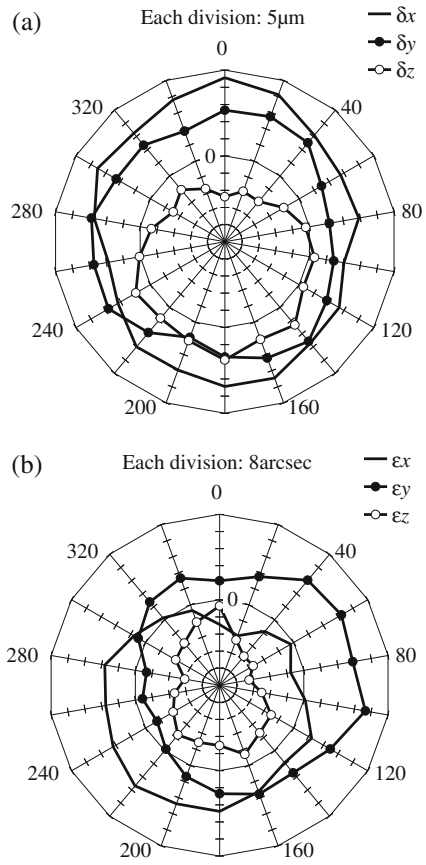

Fig. 14 Results of the geometric error components measurement for the rotary axis. **a** Displacement errors; **b** rotational errors

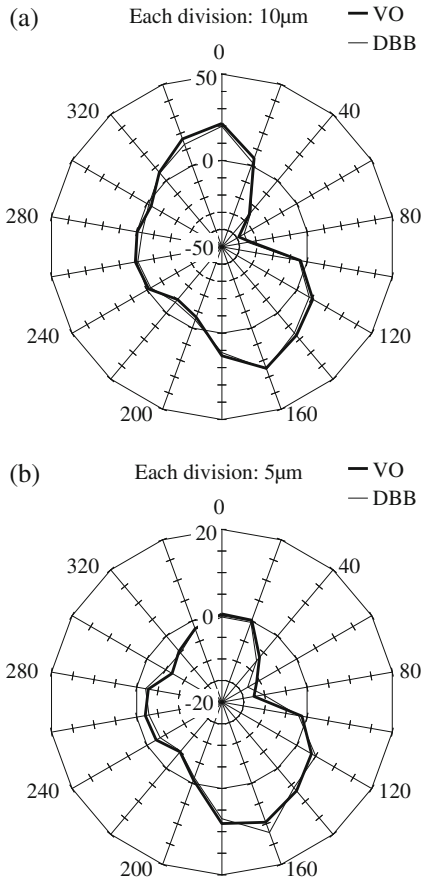

Fig. 16 Comparison of the measuring results of the two methods. **a** For point A; **b** for point B

by DBB. The coordinates of target point A is (121.779, 87.578, 59.216). The ΔLs obtained by vector operation (VO) and tested by DBB are shown in Fig. 16a. They are approximately the same at each step and the maximum deviation is about 3.64 μm when the angular displacement is 60°.

To further consolidate this verificational experiment, another target point B (49.919, 2.842, 59.216) is tested too. As shown in Fig. 16b, the ΔLs obtained by vector operation are compared with the ΔLs tested by DBB. They are approximately the same at each step and the maximum deviation is about 2.53 μm when the angular displacement is 160°.

In conclusion, the effectiveness of the three-point method for measuring the geometric error components of the rotary axis is thus verified.

6 Conclusions

A three-point method for measuring geometric error components of multi-axis machine tools by using a laser tracker is presented in this study. Since all the component errors and location errors of the linear and rotary axes can be obtained by using only one laser tracker to collect the coordinate sequence of three pre-described points, this method can be considered as a general strategy for geometric error identification of multi-axis machine tools. Experiments were carried out on a three-axis machine tool and a single rotary axis. The experimental results indicate that the identification of geometric error components is feasible by implementing the proposed method.

The proposed method has many advantages: firstly, it is simple and fast since there is no requirement for complicated equipment alignment and installation; secondly, compared to the previous laser-tracker-based method, the measuring time of the three-point method is further decreased due to the fact that only three point sequences are tested; thirdly, it is suitable for geometric error component measurements of both of linear and rotary axes, and as a result, it can be applied to calibrate multi-axis machine tools of whatever type; fourthly, all the measurement procedure are implemented in a single coordinate frame,; lastly, due to the laser tracker's capability for large-scale metrology, this method is applicable to geometric error measurement for different-sizes of machine tools, especially for large-sized machine tools.

Acknowledgments This research work was supported by the National Natural Science Foundation of China (NSFC) under NSFC Grant 60974069. The authors would like to express their appreciation to the contribution of Wang Ying and Liu Nengfeng, who are the assistant engineers at the Shenzhen Key Lab of Advanced Manufacturing Technology of Harbin Institute of Technology Shenzhen Graduate School, for offering help in experiments.

References

1. Kvrgic V, Dimic Z, Cvijanovic V, Ilic D, Bucan M (2012) A control algorithm for a vertical five-axis turning centre. Int J Adv Manuf Technol 61(5–8):569–584
2. Filho JMC (2012) Prediction of cutting forces in mill turning through process simulation using a five-axis machining center. Int J Adv Manuf Technol 58(1–4):71–80
3. Du J, Yan XG, Tian XT (2012) The avoidance of cutter gouging in five-axis machining with a fillet-end milling cutter. Int J Adv Manuf Technol 62(1–4):89–97
4. Cui GW, Lu Y, Gao D, Yao YX (2012) A novel error compensation implementing strategy and realizing on Siemens 840D CNC systems. Int J Adv Manuf Technol 61(5–8):595–608
5. Lu YX, Islam MN (2012) A new approach to thermally induced volumetric error compensation. Int J Adv Manuf Technol 62(9–12):1071–1085
6. Ashok SD, Samuel GL (2012) Modeling, measurement, and evaluation of spindle radial errors in a miniaturized machine tool. Int J Adv Manuf Technol 59(5–8):445–461
7. Zhang G, Ouyang R, Lu B, Hocken R, Veale R, Donmez A (1988) A displacement method for machine geometry calibration. CIRP Ann 37(1):515–518
8. Chen GQ, Yuan JX, Ni J (2001) A displacement measurement approach for machine geometric error assessment. Int J Mach Tools Manuf 41(1):149–161
9. Fan JW, Tian Y, Song GR, Huang XD, Kang CF (2000) Technology of NC machine error parameter identification based on fourteen displacement measurement line. J B Polytech Univ 26(6):11–15
10. Liu YW, Liu LB, Zhao XS, Zhang Q, Wang SX (1998) Investigation of error compensation technology for NC machine tool. Chin J Mech Eng 9(12):48–51
11. Wang C (2000) Laser vector measurement technique for the determination and compensation of volumetric positioning errors. Part I: basic theory. Rev Sci Instrum 71(10):3933–3937
12. Zhang HT, Yang JG, Zhang Y, Shen JH, Wang C (2012) Measurement and compensation for volumetric positioning errors of CNC machine tools considering thermal effect. Int J Adv Manuf Technol 55(1–4):275–283
13. Lau K, Ma Q, Chu X, Liu Y, Olson S (1999) An advanced 6-degree-of-freedom laser system for quick CNC machine and CMM error mapping and compensation. WIT Trans Eng Sci 23:421–434
14. Lu XD, Jamalian A (2011) A new method for characterizing axis of rotation radial error motion Part 1. Two-dimensional radial error motion theory. Precis Eng 35(1):73–94
15. Castro HFF (2008) A method for evaluating spindle rotation errors of machine tools using a laser interferometer. Measurement 41(5):526–537
16. Bryan JB (1982) Simple method for testing measuring machines and machine tools, part 1: principles and applications. Precis Eng 4(2):61–69
17. Bryan JB (1982) Simple method for testing measuring machines and machine tools, part 2: construction details. Precis Eng 4(3):125–138
18. Yang SH, Kim KH, Park YK, Lee SG (2004) Error analysis and compensation for the volumetric errors of a vertical machining centre using a hemispherical helix ball bar test. Int J Adv Manuf Technol 23(7–8):495–500
19. Zhu SW, Ding GF, Qin SF, Lei J, Zhuang L, Yan KY (2012) Integrated geometric error modeling, identification and compensation of CNC machine tools. Int J Mach Tools Manuf 52(1):24–29
20. Lee KI, Lee DM, Yang SH (2012) Parametric modeling and estimation of geometric errors for a rotary axis using double ball-bar. Int J Adv Manuf Technol 62(5–8):741–750
21. Zhang Y, Yang JG, Zhang K (2013) Geometric error measurement and compensation for the rotary table of five-axis machine tool with double ballbar. Int J Adv Manuf Technol 65(1–4):275–281

22. Liu HL, Li B, Wang XZ, Tan GY (2011) Characteristics of and measurement methods for geometric errors in CNC machine tools. Int J Adv Manuf Technol 54(1–4):195–201
23. Zhu WD, Wang ZG, Yamazaki K (2010) Machine tool component error extraction and error compensation by incorporating statistical analysis. Int J Mach Tools Manuf 50(9):798–806
24. Wang W, Kweon SH, Hwang CS, Kang NC, Kim YS, Yang SH (2009) Development of an optical measuring system for integrated geometric errors of a three-axis miniaturized machine tool. Int J Adv Manuf Technol 43(7–8):701–709
25. Liu CH, Jywe WY, Shyu LH, Chen CJ (2005) Application of a diffraction grating and position sensitive detectors to the measurement of error motion and angular indexing of an indexing table. Precis Eng 29(4):440–448
26. Park SR, Hoang TK, Yang SH (2010) A new optical measurement system for determining the geometrical errors of rotary axis of a 5-axis miniaturized machine tool. J Mech Sci Technol 24(1):175–179
27. Takatsuji T, Goto M, Kirita A, Kurosawa T, Tanimura Y (2000) The relationship between the measurement error and the arrangement of laser trackers in laser trilateration. Meas Sci Technol 11(5):477–483
28. Zhang DF, Rolt S, Maropoulos PG (2005) Modelling and optimization of novel laser multilateration schemes for high-precision applications. Meas Sci Technol 16(12):2541–2547
29. Wang JD, Guo JJ, Zhang GX, Guo BA, Wang HJ (2012) The technical method of geometric error measurement for multi-axis NC machine tool by laser tracker. Meas Sci Technol 23(4):045003
30. Umetsu K, Furutnani R, Osawa S, Takatsuji T, Kurosawa T (2005) Geometric calibration of a coordinate measuring machine using a laser tracking system. Meas Sci Technol 16(12):2466–2472
31. Went K, Schwenke H, Bosemann W, Dauke M (2002) Inspection of large CMMs by sequential multilateration using a single laser tracker. WIT Trans Eng Sci 44(6):121–130
32. Schwenke H, Franke M, Hannaford J (2005) Error mapping of CMMs and machine tools by a single tracking interferometer. CIRP Ann 54(1):475–478
33. Aguado S, Samper D, Santolaria J, Aguilar JJ (2012) Identification strategy of error parameter in volumetric error compensation of machine tool based on laser tracker measurements. Int J Mach Tools Manuf 53(1):160–169
34. Schwenke H, Schmitt R, Jatzkowski P, Warmann C (2009) On-the-fly calibration of linear and rotary axes of machine tools and CMMs using a tracking interferometer. CIRP Ann 58(1):477–480
35. Zhang ZJ, Hu H (2013) Three-point method for measuring geometric error components of linear axis and rotary axis based on sequential multilateration. J Mech Sci Technol (in press)
36. Lee JH, Liu Y, Yang SH (2006) Accuracy improvement of miniaturized machine tool: geometric error modeling and compensation. Int J Mach Tools Manuf 46(12–13):1508–1516
37. Zhang H, Zhou YF, Tang XQ, Chen JH, Shi HM (2002) Error identification and compensation of CNC machining centers using renishaw ball bar. Chin J Mech Eng 38(10):108–113